

DR RUJIE HE (Orcid ID : 0000-0003-2498-2363)

Article type : Article

## Microstructure and mechanical properties of ZrB<sub>2</sub>-SiC/Nb joints brazed with CoFeNiCrCuTi<sub>x</sub> high entropy alloy filler

Yunlong Yang<sup>1</sup>, Gang Wang<sup>1,\*</sup>, Rujie He<sup>2,\*</sup>, Da Shu<sup>1</sup>, Caiwang Tan<sup>3</sup>, Wei Cao<sup>4</sup>

<sup>1</sup> *Anhui Key Laboratory of High-performance Non-ferrous Metal Materials, Anhui Polytechnic University, Wuhu 241000, PR China*

<sup>2</sup> *Institute of Advanced Structure Technology, Beijing Institute of Technology, Beijing, 100081, China*

<sup>3</sup> *State Key Laboratory of Advanced Welding and Joining, Harbin Institute of Technology, Harbin 150001, PR China*

<sup>4</sup> *Nano and Molecular Systems Research Unit, University of Oulu, P.O. Box 3000, FIN-90014, Oulu, Finland*

*Corresponding authors: Gang Wang, Rujie He*

*E-mail addresses: gangwang@ahpu.edu.cn (G. Wang), herujie@bit.edu.cn (R. He)*

This article has been accepted for publication and undergone full peer review but has not been through the copyediting, typesetting, pagination and proofreading process, which may lead to differences between this version and the [Version of Record](#). Please cite this article as [doi: 10.1111/JACE.17732](https://doi.org/10.1111/JACE.17732)

This article is protected by copyright. All rights reserved

## Abstract

ZrB<sub>2</sub>-SiC ceramics and Nb alloy were brazed at 1160°C for 60 min with CoFeNiCrCuTi<sub>x</sub> high-entropy alloy filler. The influence of Ti content on the interface structure and mechanical properties of ZrB<sub>2</sub>-SiC/Nb joint was systematically studied. It is found that the rich-Ti Laves phase was formed due to the addition of large atomic size Ti fill into the filler alloy or brazing joint, and its content increases with Ti content. The joint brazed by high-entropy alloys filler without Ti can be divided into a tooth-shaped Cr<sub>2</sub>B reaction layer and a central area composed of a eutectic mixed structure of FCC phase and rich-Nb lamellar Laves phase. Ti and Nb are mutual solid solution elements. The increase of Ti content in the joint makes the FCC phase and the rich-Nb lamellar Laves phase to transform into a big bulk Ti-rich Laves phase and the quadrilateral (Ti, Nb)B phase. The tooth-shaped Cr<sub>2</sub>B was disappeared. The residual stress generated in the joint during the brazing process tends to cause defects such as holes and microcracks in the bulk Ti-rich brittle Laves phase. Therefore, with the addition of Ti, the normal temperature performance of the joint decreases from 216 MPa to 52 MPa. However, with the increase of Ti, the high-temperature mechanical properties of the joint first decrease, and then increase. It was mainly due to the formation of rich-Ti Laves phase and quadrilateral (Ti, Nb)B with excellent high-temperature mechanical properties. When brazing with CoFeNiCrCuTi<sub>1.5</sub> filler, the high temperature performance of the joint reached 92% of its room temperature performance.

## Keywords

ZrB<sub>2</sub>-SiC ceramic; Nb alloy; High temperature filler; brazed

## 1. Introduction

Ceramics have excellent physical, chemical and high temperature properties and have been widely used as thermal structure materials in aerospace [1]. Ceramics are required to joining to metals, such as Ni-based alloy [2], Nb [3, 4] and Ti-based alloy [5], in order to achieve a component endowed with merits of metal and ceramic properties. Among the technologies of joining ceramics and metals, brazing is considered to be an efficient, high-quality and simple effective method [6].

Due to the inherent physical and chemical properties of ceramics and metals, there are some basic problems need to be considered. Metal is difficult to wet ceramic because of the different bond-type matching problems between ceramics and metals. The difference in coefficients of thermal expansion (CTE) between metals and ceramics is large, and residual stress or even crack is easily generated at the interface [7]. Researchers have conducted a lot of research on brazing process optimization, interface physics and metallurgical coordination, and composite brazing filler [8-15]. In terms of filler design and prepare, Huang et al. brazed  $C_f/SiC$  ceramics with TC4 alloy by using Ti-based alloy filler. An obvious reaction layer was formed due to the reaction between active Ti, Zr element and C, Cu, Ni [8]. Feng *et al.* study the microstructure evolution of TiAl alloy and  $C_f/SiC$  ceramic with Ag-Cu-xTi alloys as filler through brazing process optimization [10]. By adding particle phase, soft metal foil interlayer, foam metal and active elements in the filler, the residual stress in the joint can be reduced and a high-quality joint can be obtained. In order to relieve the residual stress of the joint and obtained a high-quality joint, particulate phase, soft metal foil interlayer, foam metals and active elements were introduced. Ban *et al.* [14] used a mixed powder of Cu, Ti and graphite to join SiC ceramic to Ti-based alloy. Chen *et al.* prepared a  $C_f/SiC$  composite ceramic with porosity and performed densification after joining. The wettability between the brazing filler metal and the ceramic is improved, and the filler melts penetrates into the matrix of composite, which increases the wetting contact area and enhances the strength of the joint [15]. In view of the above studies, adding active elements into the brazing filler can reduce the wetting angle and achieve a good wettability of the joint interface, and therefore obtain high-performance ceramic and metal brazed joints.

In the traditional active filler system, Ni-Ti active filler is regarded as one of the choices of high temperature filler due to its excellent high temperature performance. However, when brazing with Ni-Ti high-temperature brazing filler metal, it is easy to generate a large amount of brittle intermetallic compounds at the interface, resulting in greater residual stress and reducing joint

performance. Qi *et al.* [16] successfully realized the SiC ceramics using Ni-Ti filler metal. The study found that the Ti<sub>2</sub>Ni phase generated at the interface has a very high coefficient of thermal expansion (CTE), and the residual stress caused by the CTE mismatch between Ti<sub>2</sub>Ni and SiC is not conducive to the shear strength of the joint. At 600°C, the shear strength of the joint is only 36 MPa, which is 52% of the room temperature shear strength. Zhang *et al.* [17] successfully brazed Si<sub>3</sub>N<sub>4</sub> ceramics with Ni-Au-V filler and evaluated the high-temperature mechanical properties of the joint. The study found that a large number of brittle Ni-rich phases appeared in the joint, which reduced the performance of the joint. At 800°C, due to the softening of the metal in the joint, the shear strength of the joint is only 35% of the room temperature shear strength. As a new type of alloy system, high-entropy alloys have thermodynamically high-entropy effects that will promote the mixing of elements, easily form body-centered or face-centered cubic solid solution structures, thereby inhibiting the formation of brittle metal compounds; kinetic high-entropy alloys. During the solidification process, the separation and diffusion process between the elements is very slow, leading to delays in nucleation and growth, making the interface microstructure tend to be nano-sized, and its resistance to high temperature tempering is excellent [18]. If used as a brazing filler metal, its unique thermodynamic and kinetic properties are positive for inhibiting the excessive dissolution of the base metal and filler elements during the brazing process, reducing the generation of harmful substances at the interface, and improving the solid solution strengthening ability of the joint. Based on our previous research, a high-quality joint of SiC ceramics was achieved with the CoFeNiCrCu high-entropy alloy as filler [19]. Thanks to the high entropy effect of CoFeNiCrCu filler, the joints was mainly composed of random solid solutions and have excellent shear properties. During the formation of joint, the loss of elements from HEA alloy may indeed lead to the damage of solid solution. In order to solve this problem, a new filler based on HEA are under design and preparation. The key idea is to add a Ti in the HEA filler. The reasons are follows. Firstly, Ti is more active than Cr. The mixing enthalpy between Ti and B is -160kJ/mol [20]. So, Ti element can stabilize Cu element and even Cr element in CoFeCrNiCu HEA, which can maintain the composition and microstructure of CoFeCrNiCu HEA. Secondly, as an active element, Ti can improve the wetting of the ZrB<sub>2</sub>-SiC interface and is beneficial to the metallurgical reaction of the joint. Finally, it is reported that the CoFeCrNiCuTi<sub>x</sub> alloy with small addition of Ti is still HEA alloy system [21]. Therefore, in the present work, active element of Ti was added into CoFeNiCrCu alloy to prepare a CoFeNiCrCuTi<sub>x</sub> (x=0, 0.5, 1.5, x values in molar ratio) filler system and the weldability of high entropy CoFeNiCrCu alloy filler system was

studied. A systematically research was conducted to investigated the influence of  $\text{CoFeNiCrCuTi}_x$  filler on shear property of brazed joints.

## 2. Experimental

$\text{ZrB}_2$ -20vol% SiC ceramic (with density of  $4.93\text{g/cm}^3$ ), i.e. 90 % as compared to the fully dense material, was provided by Harbin Institute of Technology. Nb plate with a purity of 99.95 % was used as the metal substrate. The dimensions of  $\text{ZrB}_2$ -SiC ceramic and Nb for brazing were  $4\text{mm}\times 4\text{mm}\times 4\text{mm}$  and  $10\text{mm}\times 10\text{mm}\times 4\text{mm}$ , respectively. The  $\text{CoFeNiCrCuTi}_x$  ( $x=0, 0.5, 1.5, x$  values in molar ratio) high entropy alloy were prepared by arc melting technology. The master alloys were re-melted 4 times to reach compositional homogeneity in a Ti-gettered argon atmosphere and then cast into a copper mould to form rod samples with 6 mm in diameter. Then, the  $\text{CoFeNiCrCuTi}_x$  alloy was cut into 0.6 mm and carefully polished to 0.4 mm with SiC sandpaper.  $\text{ZrB}_2$ -SiC ceramics and Nb alloys were also cut and polished with the same specifications of SiC sandpaper after on-line cutting, so that the surface to be welded on the substrate was tightly combined with the filler during assembly.

Before brazing, ceramics, metals and fillers were ultrasonically cleaned in acetone for 10 min. Brazing process was performed at  $1160^\circ\text{C}$  with a heating rate of  $10^\circ\text{C/min}$  and holding for 60 min in a vacuum brazing furnace (JVL211) with a pressure  $< 6.0\times 10^{-3}$  Pa. The brazed samples were cooled down at a rate of  $5^\circ\text{C/min}$  to  $300^\circ\text{C}$ , and then naturally to the room temperature in the furnace.

The microstructure and phase of brazed joint was characterized by scanning electron microscope (SEM, SU-8010), equipping with an energy-dispersive X-ray spectrometer (EDS) and X-ray diffractometer (XRD, D-MAX Rapid II Cu  $K\alpha$ ). Shear strength of joints were measured on an Instron 5500 machine. The measurements were done three times to obtain an average value.

## 3. Results and discussion

Figures 1 and Table 1 depicts the microstructure and EDX analysis of as-cast  $\text{CoFeNiCrCuTi}_x$  alloy filler, respectively. The  $\text{CoFeNiCrCu}$  alloy depicts a dendritic microstructure, as shown in Fig. 1(a). Because of its higher electronegativity than other elements, Cu element is less stable in FCC1 dendrites and is easily repelled into the interdendritic region. The result agrees well with our previous research [16]. Compared with the  $\text{CoFeNiCrCu}$  alloy, the microstructure of the  $\text{CoFeNiCrCuTi}_{0.5}$  alloy has undergone obviously changes, the

dendritic structure disappears and a small light grey cluster phase and an elliptical white phase are formed, as shown in Fig. 1(b). According to EDX analysis of  $\text{CoFeNiCrCuTi}_{0.5}$  and previous research [21], the light grey phase rich of (Ni, Ti) could be another FCC solid solution, and the white phase was the  $\text{Cu}(s, s)$ . The light grey FCC phase is named FCC2. When the Ti content was increases to 16.7 at. % ( $x=1$ ), compared with the  $\text{CoFeNiCrCuTi}_{0.5}$  alloy, the original FCC phase disappeared and replaced by a large amount of eutectic structure composed of light gray phase, black phase phase, gray phase, and white phase, as show in Fig. 1(c). According to EDX analysis of  $\text{CoFeNiCrCuTi}$ , the light grey phase is a (Ni, Ti)-rich phase, the black phase is a (Ti, Co)-rich phase, the grey phase is a (Cr, Fe)-rich phase, the white phase is a Cu-rich phase. It can be inferred as FCC2 phase,  $\sigma$  phase, Laves phase and  $\text{Cu}(s, s)$  phase, respectively. Shun *et al.* [22] investigated the microstructure and mechanical properties of  $\text{CoFeCrNiTi}_x$  alloys with different Ti content. It can be observed that the microstructures of the  $\text{CoFeCrNiTi}$  alloy were compose of the rich-(Ni, Ti) phase, rich-(Cr, Fe)  $\sigma$  phase and (Ti, Co)-rich Laves phase. Therefore, it can be confirmed that the (Cr, Fe)-rich phase, (Ti, Co)-rich phase, (Ni, Ti)-rich phase and Cu-rich phase are  $\sigma$  phase, Laves phase, FCC2 phase and  $\text{Cu}(s, s)$  phase, respectively [22]. When the Ti content was increases to 23 at. % ( $x=1$ ), the  $\sigma$  phase and eutectic structure disappear, a large number of dendritic Laves phases are formed, and the intergranular region is mainly composed of FCC2 phase and Cu phase. In addition, a small amount of new black phase is formed in the intergranular region, as show in Fig. 1(d). The new black phase is mainly composed of Cr element. The newly formed light black phase is inferred as Cr phase. Cr is an unstable element, tending to accumulate and precipitating between dendrites [23]. The XRD analysis results of  $\text{CoCrFeNiCuTi}_x$  alloy are consistent with the above conclusions, as show in Fig. 2.

Fig. 3 shows the typical cross-sectional SEM image and EDS elemental mappings of the  $\text{ZrB}_2$ -SiC/Nb brazed joint obtained at  $1160^\circ\text{C}$  for 60 min using  $\text{CoCrFeNiCu}$  filler. As shown in Fig. 3(a), a defect-free joint with a thickness of about  $150\mu\text{m}$  is obtained by brazing with  $\text{CoCrFeNiCu}$  filler. It can be found that there are two characteristic areas in the joint, namely the reaction layer (Zone I) and the central area (Zone II). The Co, Fe, Ni, Cu, Nb and other elements are evenly distributed in the Zone II, as shown in Fig. 3(c)-(g). Among them, Nb element mainly exists in the gray lamellar structure, occupying the large area of the Zone II. The Zone I is mainly composed of Cr and B elements, as shown in Fig. 3(h)-(i).

Fig. 4 shows the SEM image of typical interface microstructure of  $\text{ZrB}_2$ -SiC/Nb joint brazed at  $1160^\circ\text{C}$  for 60 min with  $\text{CoCrFeNiCu}$  filler. It can be found that the Zone I was tooth-like and

closely combined with the Zone II, and the Zone II was mainly composed of gray lamellar structure, as shown in Fig. 4(a). Fig. 4(b)-(d) were enlarged views of Zone I, Zone II and the interface structure with Nb alloy, respectively. It can be found that a continuous tooth shape interface reaction layer with a thickness of about 50 $\mu$ m was formed between the ZrB<sub>2</sub>-SiC ceramic and the joint, which was mainly composed of black phase A, as shown in Fig. 4(b). The formation of the reaction layer effectively shows the chemical metallurgical connection between the ZrB<sub>2</sub>-SiC ceramic and the joint. Fig. 4c and Fig. 4d show the morphology of feature area II and its interface with Nb alloy. Zone II was mainly composed of the eutectic structure of gray phase B and brown phase C. There are small amount of light gray phase D, dark gray phase E and black phase F between gray phases B. The light white phase G exists near the interface of the Nb alloy. To identify the phases A-G in the joint, the chemical compositions of the phases were listed in Table 2. Based on Fe-Cr-C-B ternary phase diagrams [24], the phase A derived mainly from Cr and B could be corresponds to Cr<sub>2</sub>B. Due to the diffusion of boron atoms in two borides that do not have cubic crystal symmetry, tooth-like Cr<sub>2</sub>B dentate borides were formed [25]. Phase B was an Nb-rich phase, phase C was composed of Co, Fe, Cr, Ni, and its composition was highly similar to the Laves phase and FCC phase which reported by Filip [26]. The main reason for the formation of Laves phase was due to the large amount of Nb alloy dissolved in the liquid filler during the brazing process. The radius of Nb was larger than other elements and cause serious lattice distortion, which made the FCC phase transform to the Laves phase [26]. Phase D mainly contains Cr and B, Phase E mainly contains Cr, Fe and B, and the element stoichiometric ratios were nearly 5:1:3 and 2:1, respectively. Combined with Fe-Cr-C-B binary phase diagram [24], phase D and E could be (Cr, Fe)<sub>2</sub>B and Cr<sub>2</sub>B. The light gray phase F was mainly composed of Cu elements and presumed it to be the Cu(s, s) phase. Due to Cu atoms were unstable element, it was easy to precipitate between the crystals to form Cu(s, s) [19]. The chemical composition of phase G was mainly composed of Nb element, indicating that the layer between zone II and Nb alloy was Nb(s, s) phase [27]. Through the above analysis, it can be obtained that the A-G phases in the brazed joint are Cr<sub>2</sub>B, Laves, FCC, (Cr, Fe)<sub>2</sub>B, Cr<sub>2</sub>B, Cu(s, s), and Nb(s, s).

Fig. 5 shows the microstructure and main elements distribution of the ZrB<sub>2</sub>-SiC/Nb joint brazed using CoCrFeNiCuTi filler at 1160 $^{\circ}$ C for 60 min. As shown in Fig. 5(a), the microstructure of the joint is composed of two characteristic zones: Zone I (interfacial reactive layer) and Zone II (the brazed seam), respectively. A microcrack is detected in the Zone II. Zr element is mainly distributed in ZrB<sub>2</sub>-SiC ceramic base material, as show in Fig. 5(c). The Co, Fe, Ni, Cu, Nb and Ti

are extensively distributed in the middle of the joint, as show in Fig. 5(c)-(h). The Cr element is mainly segregated in the Zone I, as show in Fig. 5(i).

The BSE images of the  $ZrB_2$ -SiC/CoCrFeNiCuTi/Nb joint brazed at 1160°C for 60 min are shown in Fig. 6. It can be seen from Fig. 6(a) that the total thickness of the joint was about 80  $\mu$ m. To identify the phases A-G in the joint, the chemical compositions of the phases were listed in Table 3. It could be clearly observed in Fig. 6(b) that phases A and B were located in the Zone I. Phases A mainly containing elements Cr and B, and the ratio was nearly 2:1. Phase C mainly contains Cr, Co, Fe and Ni, and the element stoichiometric ratios were nearly 1:1:1:1. Chang *et al.* [28] used the laser cladding method to prepare FeCrCoNiB high-entropy alloy coatings with different Cr contents on the surface of AISI 1045 alloy, and reported the microstructure of the coatings with different Cr contents. The results show that the coating is mainly composed of FCC phase and Cr-B compound. When  $x>0.5$ , the borides generated in the coating are mainly  $Cr_2B$  phase. Therefore, the phase A and the phase C were identified as  $Cr_2B$  phase and FCC phase. The phase B and F was mainly formed by the Ti, Nb and B, and ascribed to (Ti, Nb)B. It was similar to the research of Ding *et al.* [29].

It could be clearly observed that phases C, D, E and F were located in the Zone II, as show in Fig. 6(c). The elements Cr, Co, Fe, Ni and Nb were detected in phase D, and the stoichiometry of Cr: Co: Fe: Ni: Ti ratio in atomic percent was close to 1:1:1:1:1. It could be rich-Ti Laves. The phase E was mainly composed of Cu elements. Combining the ratios, the phase D and phase E could be the rich-Ti Laves phase and Cu(s, s) phase [16]. It can be found that a transition layer mainly composed of phase G was formed near the Nb alloy interface, as show in Fig. 6(d). According to the EDS analysis of phase G and previous research [27], the phase G was identified as the Nb(s, s) phase which mainly composed of Nb elements. The typical interfacial microstructure of the  $ZrB_2$ -SiC/Nb joint brazed with CoCrFeNiCuTi at 1160°C for 60 min was  $ZrB_2$ -SiC/ $Cr_2B$ +(Ti, Nb)B/FCC+rich-Ti Laves+(Ti, Nb)B+Cu(s,s)/Nb(s, s)/Nb.

Fig. 7 shows the effects of Ti content on the average shear strength of  $ZrB_2$ -SiC/Nb brazed joints at room temperature and temperature of 650°C. After adding Ti, the joint shows poor performance. At room temperature, the shear strength of the joint without Ti was ~216MPa, and gradually decreased with the increase of Ti content, down to ~58MPa ( $x=1$ ), a decrease of 73%. At 650°C, the shear strength of the joint without Ti is ~94MPa, and it first decreases and then increases as the Ti content increases. When the Ti content was increases to 23 at. % ( $x=1$ ), the shear strength of the joint is ~50MPa, which is only reduced by 14% relative to the shear strength

at room temperature. It was higher than the high temperature shear strength of conventional Ni-Ti high temperature filler brazed joints [16].

Fig. 8 depicts the effects of Ti content in the filler metal on the the microstructure of the ZrB<sub>2</sub>-SiC/Nb brazed joints. It could be clearly found that although two characteristic zones can be observed in all joints obtained by different Ti content filler, but the interface microstructure of two zones in the joints has a significantly different. For the CoCrFeNiCu filler without Ti addition, a homogeneous brazed joint with defect-free was observed, as shown in Fig. 8(a). At this time, the reaction layer of the joint is in a continuous tooth shape, mainly composed of Cr<sub>2</sub>B phase, and the width of the reaction layer was ~ 50 μm. Compared with the FCC phase and Cu(s, s) phase initial structure of CoCrFeNiCu filler, the central area of the joint was mainly composed of lamellar rich-Nb Laves phase, and a small amount of mixed eutectic microstructure such as FCC phase, Laves phase and Cu(s, s) phase also distributed in it. Liu *et al.* [30] systematically investigated the influence of the addition of Nb on the CoCrCuFeNiNb HEA structure evolution and mechanical properties. The results show that the addition of Nb, which has a large difference in atomic size from other elements, will cause severe lattice distortion, thereby promoting the phase transition from FCC to Nb-rich Laves phase. The continuous tooth-shaped reaction layer can promote the close bonding between the weld and the substrate, and lamellar rich-Nb Laves phase has excellent mechanical properties no matter at room temperature or high temperature. He *et al.* reported the effect of different content of Nb in CoCrFeNiNb eutectic alloy. The research found that the addition of Nb will make the lamellar rich-Nb Laves phase formed. The structure of the layered Nb-rich Laves phase is still stable at 900°C and shows excellent mechanical properties [31]. Therefore, the room temperature shear strength of the joint was 216MPa. When tested at 650°C, the high temperature shear strength of the joint reached to 94MPa. With the Ti addition in the filler material, the microstructure and mechanical properties of the joint changes greatly. When the Ti content was increases to 9.9 at. % ( $x = 0.5$ ), the tooth-shaped Cr<sub>2</sub>B layer was disappears, the reaction layer is mainly composed of (Ti, Nb)B and Cr<sub>2</sub>B phases, and the thickness of the reaction layer is reduced to 20μm, as shown in Fig. 8(b). It was observed that the joints with or without Ti addition both contain a small amount of FCC phase, but due to the addition of Ti, the central area of the joint changed from a lamellar rich-Nb Laves phase layer to a big connected Ti/Nb-rich Laves phase double-layer structure. At the same time, because of the large brittle Laves phase formation that defects such as cracks and cavity formed in the joint, which makes the shear strength of the joint significantly reduced. However, due to the high thermal stability of the Laves

phase, its high temperature shear strength is close to 68% of the normal temperature shear strength [32]. When the Ti content was increased to 16.7 at. % ( $x=1$ ), compared with the joint with low Ti content, it can be clearly observed from Fig. 8(c) that defects such as cracks were also obtained in the joint, the (Ti, Nb)B phase in the reaction layer increases, and the thickness of the reaction layer increases to 25 $\mu\text{m}$ . The central area of the joint which was rich-Ti/Nb Laves phase double-layer becomes a single Ti-rich Laves phase layer, and a large amount of (Ti, Nb) B phase was formed. It was probable due to the close atomic size of Ti and Nb, which can be dissolved in each other [33]. As Ti content increases, the transformation of the rich-Nb Laves phase to the rich-Ti Laves phase. Zhang *et al.* [34] reported the variation of Gibbs free energy of carbides and borides with temperature and found that compared to  $\text{Cr}_2\text{B}$ , TiB has the greatest tendency to form due to its lower Gibbs free energy at 1160 $^\circ\text{C}$ , while Ti and Nb can be dissolved in each other, and the (Ti,Nb)B phase was thus formed. Therefore, compared with the joint with low Ti content, the normal temperature performance of the joint with higher Ti content remains unchanged, and the high temperature performance is improved to a certain extent. It was due to the formation of the high temperature toughening phase (Ti, Nb)B, which was in line with the reported form Ref [35]. With the further increase of Ti addition, the number of (Ti, Nb) B phase and Ti-rich Laves phases is further increased. When the Ti content was  $\sim 23\text{at.}\%$  ( $x=1.5$ ), the FCC phase in the central area of the joint disappears, and the generation of (Ti, Nb) B phase and Ti-rich Laves phase increases. In the joint reaction,  $\text{Cr}_2\text{B}$  disappeared, (Ti, Nb) B phase was formed in large quantities, a new phase  $\text{Cr}_2\text{Ti}$  was formed. The thickness of the reaction layer increased to 30  $\mu\text{m}$ , as shown in Fig. 8(d). In this moment, the normal temperature shear strength of the joint was further reduced to 52 MPa, and the high temperature shear strength was increased to 48 MPa, which is close to the normal temperature shear strength of the joint. It was beneficial to the large-scale formation of the Laves phase with strong high temperature stability and the high temperature tough phase (Ti, Nb)B. The above conclusion was supported by the XRD results in Fig. 9.

The shear fracture surface of ceramic-metal joints can be used to determine whether there is a large amount of residual stress in the joint [35]. In order to further verify the relationship between the strength of the  $\text{ZrB}_2\text{-SiC/Nb}$  joint and the interface structure with Ti addition. After the shear test, the fracture surfaces of the joints under different content of Ti were analyzed by SEM, and the results are shown in Fig. 10. For the joint brazed without Ti addition, whether it was tested at room temperature or high temperature, the crack initiates from the ceramics/filler metal layer interface, and then extends into the ceramic substrate which was far away from the joint, leaving a

typical curved fracture, as shown in Fig. 10(a) and (e). With the addition of Ti, whether the test was performed at room temperature or high temperature, the cracks start from the ceramic/filler metal layer interface and then extend to the ceramic substrate near the joint, causing the ceramic substrate to peel off, and the fracture surface was relatively flat, as shown in Fig. 10(b)-(d) and (g)-(h). It was possible due to the increasing amount of bulk Laves phase with the addition of Ti, resulting in larger residual stress at the ceramic/filler metal layer interface, causing microcracks in the ceramic near the joint.

#### 4. Conclusions

The effect of Ti content on the microstructure of CoFeNiCrCuTi<sub>x</sub> high-entropy alloy fillers and the microstructure and mechanical properties of ZrB<sub>2</sub>-SiC/Nb brazed joints brazed with CoFeNiCrCuTi<sub>x</sub> high-entropy alloy fillers with different Ti content are investigated in this paper.

- 1) The addition of Ti will make the filler change from a single FCC phase to a mixture of Ti-rich Laves phase and FCC2 phase. With the Ti element increases, the number of Ti-rich Laves phases in the filler alloy gradually increases.
- 2) The typical interface microstructure of ZrB<sub>2</sub>-SiC/CoFeNiCrCuTi/Nb joint brazed at 1160°C for 60 min is: ZrB<sub>2</sub>-SiC/Cr<sub>2</sub>B+(Ti, Nb)B/FCC+rich-Ti Laves+(Ti, Nb)B+Cu (s, s)/Nb( s, s)/Nb.
- 3) The addition of Ti result the formation of large rich-Ti Laves intermetallic compounds in the joint. With the addition of Ti, the central area of the joint changes from the mixed eutectic structure of the layered FCC phase and rich-Nb Laves phase without Ti to the mixed structure of the bulk rich-Ti Laves, FCC phase and (Ti, Nb)B phase. The reaction layer of the joint changes from the tooth-shaped Cr<sub>2</sub>B reaction layer without Ti to a mixed structure of Cr<sub>2</sub>B and (Ti, Nb)B, and the thickness was reduced to 20μm.
- 4) When tested at room temperature, as Ti increases, the shear strength of the joint gradually decreases. When brazing with CoFeNiCrCuTi<sub>1.5</sub> filler, the minimum shear strength is 52 MPa. When tested at 650°C, with the increase of Ti, the shear strength of the joint first decreased and then stabilized, and its high temperature stability continued to increase. When brazing with CoFeNiCrCuTi<sub>1.5</sub> filler, the high temperature performance of the joint was close to its performance at room temperature.

#### Acknowledgement

This work was financially supported by the Natural Science Foundation of Anhui Province [2008085J23], National Natural Science Foundation of China [51704001]; Talent Project of Anhui Province [Z175050020001]; Anhui Provincial Grant for high-level platform construction, and the Academy of Finland [No. 311934].

## References

1. Shirzadi AA, Zhu Y, Bhadeshia HKDH. Joining ceramics to metals using metallic foam. *Mater Sci Eng A*. 2008; 496: 501-506.
2. Zhang LX, Shi JM, Li HW, Tian XY, Feng JC. Interfacial microstructure and mechanical properties of ZrB<sub>2</sub>-SiC-C ceramic and GH99 superalloy joints brazed with a Ti-modified FeCoNiCrCu high-entropy alloy. *Mater Des*. 2016; 97: 230-238.
3. Sun Y, Zhang J, Liu CF. Microstructure and formation mechanism of C<sub>f</sub>/SiC and Nb joint brazed with laminated amorphous Ti-Zr-Cu-Ni/crystalline Ti composite filler. *Vacuum*. 2020; 179: 109480.
4. Yang ZW, Wang CL, Han Y, Zhao YT, Wang Y, Wang DP. Design of reinforced interfacial structure in brazed joints of C/C composites and Nb by pre-oxidation surface treatment combined with in situ growth of CNTs. *Carbon*. 2019; 143: 494-506.
5. Wang G, Wang ZT, Wang W, He RJ, Gui KX, Tan CW, Cao W. Microstructure and shear strength of ZrB<sub>2</sub>-SiC/Ti-6Al-4V joint by TiCuZrNi with Cu foam. *Ceram Int*. 2019; 45: 10223-10229.
6. Chen B, Xiong HP, Cheng YY, Mao W, Wu SB. Microstructure and property of AlN joint brazed with Au-Pd-Co-Ni-V brazing filler. *J Mater Sci Technol*. 2015; 31: 1034-1038.
7. Zhang J, Liu JY, Wang TP. Microstructure and brazing mechanism of porous Si<sub>3</sub>N<sub>4</sub>/Invar joint brazed with Ag-Cu-Ti/Cu/Ag-Cu multi-layered filler. *J Mater Sci Technol*. 2018; 34: 713-719.
8. Cui B, Huang HJ, Cai C, Chen SH, Zhao XK. Microstructures and mechanical properties of C<sub>f</sub>/SiC composite and TC4 alloy joints brazed with (Ti-Zr-Cu-Ni)+W composite filler materials. *Compos Sci Technol*. 2014; 97: 19-26.
9. Wang WL, Fan DY, Huang JH, Li CL, Chen SH. Microstructural mechanism and mechanical properties of C<sub>f</sub>/SiC composite/TC4 alloy joints composite-diffusion brazed with TiZrCuNi+TiC<sub>p</sub> composite filler. *Mater Sci Eng A*. 2018; 728: 1-9.
10. Yang ZW, He P, Feng JC. Microstructural evolution and mechanical properties of the joint of

- TiAl alloys and C<sub>f</sub>/SiC composites vacuum brazed with Ag-Cu filler metal. *Mater Charact.* 2011; 62: 825-832.
11. Wan P, Li M, Xu K, Wu HB, Chang KK, Zhou XB, Ding XD, Huang ZG, Huang Q. Seamless joining of silicon carbide ceramics through an sacrificial interlayer of Dy<sub>3</sub>Si<sub>2</sub>C<sub>2</sub>. *J Eur Ceram Soc.* 2019; 39: 5457-5462.
  12. Zhang Q, Sun LB, Liu QY, Zhang J, Liu CF. Effect of brazing parameters on microstructure and mechanical properties of C<sub>f</sub>/SiC and Nb-1Zr joints brazed with Ti-Co-Nb filler alloy. *J Eur Ceram Soc.* 2017; 37: 931-937.
  13. Wang WL, Wang YL, Huang JH, Yu RH, Chen SH. Joining of C<sub>f</sub>/SiC composite and stainless steel via Ag+Ti filler in-situ alloying. *J Manuf Process.* 2019; 274: 116295.
  14. Ban YH, Huang JH, Zhang H, Zhao XK, Zhang ZY. Microstructure of reactive composite brazing joints of C<sub>f</sub>/SiC composite to Ti-6Al-4V alloy with Cu-Ti-C filler material. *Rare Metal Mat. Eng.* 2009; 38: 713-716.
  15. Chen XG, Xie RS, Lai ZW, Liu L, Yan JC. Interfacial structure and formation mechanism of ultrasonic-assisted brazed joint of C<sub>f</sub>/SiC ceramics with Al-12Si filler metals in air. *J Mater Sci Technol.* 2017; 33: 492-498.
  16. Qi Q, Zhang J, Hu HW, Lu CG. Benefits of Zr additive element in the Ti<sub>24</sub>Ni eutectic filler in vacuum brazing of SiC ceramics. *Vacuum.* 2019; 162(1): 110-113.
  17. Zhang J, Sun Y, Liu CF, Zhang HW. Interfacial microstructure of Si<sub>3</sub>N<sub>4</sub>/Si<sub>3</sub>N<sub>4</sub> joint brazed using Au-Ni-V filler alloy. *J Mater Sci.* 2010; 45(8): 2188-2193.
  18. Wang S, Chen Z, Feng LC, Liu YY, Zhang P, He YZ, Meng QQ, Zhang JY. Nano-phase formation accompanying phase separation in undercooled CoCrCuFeNi-3at. % Sn high entropy alloy. *Mater Charact.* 2018; 144: 516-521.
  19. Wang G, Yang YL, He RJ, Tan CW, Huttula M, Cao W. A novel high entropy CoFeCrNiCu alloy filler to braze SiC ceramics. *J Eur Ceram Soc.* 2020; 40: 3391-3398.
  20. Zhang M, Wang XH, Liu SS, Qu KL. Microstructure and high-temperature properties of Fe-Ti-Cr-Mo-B-C-Y<sub>2</sub>O<sub>3</sub> laser cladding coating. *J Rare Earth.* 2020; 38: 683-688.
  21. Wang XF, Zhang Y, Qiao Y, Chen GL. Novel microstructure and properties of multicomponent CoCrCuFeNiTi<sub>x</sub> alloys. *Intermetallics.* 2008; 15: 357-362.
  22. Shun TT, Chang LY, Shiu MH. Microstructures and mechanical properties of multiprincipal component CoCrFeNiTi<sub>x</sub> alloys. *Mater Sci Eng A.* 2012; 556: 170-174.
  23. Li QH, Yue TM, Guo ZN, Lin X. Microstructure and Corrosion Properties of AlCoCrFeNi

- High Entropy Alloy Coatings Deposited on AISI 1045 Steel by the Electrospark Process. *Metall Mater Trans A*. 2013; 44: 1767-1778.
24. Roettger A, Lentz J, Theisen W. Boron-alloyed Fe-Cr-C-B tool steels-Thermodynamic calculations and experimental validation. *Mater Des*. 2015; 88: 420-429.
  25. Brakman CM, Gommers AWJ, Mittemeijer EJ. Boring of Fe and Fe-C, Fe-Cr and Fe-Ni alloys; Boride-layer growth kinetics. *J Mater Res*. 1989; 4: 1354-1370.
  26. Filip P, Marcello C, Alexandra S, Vojtěch K, Zbyněk V, Andrea S, Dalibor V, Jana C, Jaroslav C. High-strength ultrafine-grained CoCrFeNiNb high-entropy alloy prepared by mechanical alloying: Properties and strengthening mechanism. *J Alloy Compd*. 2020; 835: 155308.
  27. Li C, Huang CY, Chen L, Si XQ, Chen Z, Qi JL, Huang YX, Feng JC, Cao J. Microstructure and mechanical properties of the SiC/Nb joint brazed using AgCuTi+B<sub>4</sub>C composite filler metal. *Int J Refract Met H*. 2019; 85: 105049.
  28. Chang F, Zhang C, Huang B, Li S, Dai PQ. Thermal stability and oxidation resistance of FeCr<sub>x</sub>CoNiB high-entropy alloys coatings by laser cladding. *Surf Coat Tech*. 2019; 359: 132-140.
  29. Ding RG, Jones IP, Jiao HS. Effect of carbon on the microstructures and mechanical properties of as cast Nb-base alloy. *Mater Sci Eng A*. 2008; 485: 92-98.
  30. Liu ZQ, Chen J, Huang ZP, Yu MD. Microstructures and mechanical properties of Nb-alloyed CoCrCuFeNi high-entropy alloys. *J Mater Sci Technol*. 2018; 34: 365-369.
  31. He F, Wang ZJ, Shang XL, Leng C, Li JJ, Wang JC. Stability of lamellar structures in CoCrFeNiNb<sub>x</sub> eutectic high entropy alloys at elevated temperatures. *Mater Des*. 2016; 104: 259-264.
  32. Liu WH, Yang T, Liu CT. Precipitation hardening in CoCrFeNi-based high entropy alloys. *Mater Chem Phys*. 2018; 210: 2-11.
  33. Gao Y, Liu ZD, Liu CC. Room and high-temperature mechanical properties of ZrB<sub>2</sub>-based composite alloyed with Ti and refractory metal Nb. *Int J Refract Met H*. 2021; 94: 105387.
  34. Zhang M, Wang XH, Liu SS, Qu KL. Microstructure and high-temperature properties of Fe-Ti-Cr-Mo-B-C-Y<sub>2</sub>O<sub>3</sub> laser cladding coating. *J Rare Earth*. 2020; 38: 683-688.
  35. Park JW, Mendez PF, Eagar TW. Strain energy distribution in ceramic-to-metal joints. *Acta Mater*. 2002; 50: 883-899.

## Table captions

Table 1 Results of EDS of CoFeNiCrCuTi<sub>x</sub> (at. %)

Table 2 Results of EDS at points A~G in Fig. 4 (at. %)

Table 3 Results of EDS at points A~G in Fig. 7 (at. %)

## Figure captions

Fig.1 Microstructure of the CoFeNiCrCuTi<sub>x</sub> alloys (x=0, 0.5, 1 and 1.5, x values in molar ratio): (a) Ti<sub>0</sub> (b) Ti<sub>0.5</sub> (c) Ti (d) Ti<sub>1.5</sub>

Fig.2 XRD analysis of CoCrFeNiCuTi<sub>x</sub> alloy

Fig. 3 Microstructure and EDS maps of ZrB<sub>2</sub>-SiC/Nb joint with CoCrFeNiCu filler: a) SEM of joint; b) to i) the distribution of different elements

Fig. 4 The SEM image of typical interface microstructure of ZrB<sub>2</sub>-SiC/Nb joint brazed at 1160°C for 60 min with CoCrFeNiCu filler: (a) the whole interface (b) Zone I (c) Zone II (d) Nb alloy and zone II interface

Fig. 5 Microstructure and EDS maps of brazed joint with CoCrFeNiCuTi filler: a) SEM of joint; b) to i) the distribution of different elements

Fig. 6 The SEM image of typical interface microstructure of ZrB<sub>2</sub>-SiC/Nb joint brazed at 1160°C for 60 min with CoCrFeNiCuTi filler: (a) the whole interface (b) Zone I (c) Zone II (d) Nb alloy and zone II interface

Fig. 7 Shear strength of ZrB<sub>2</sub>-SiC/CoCrFeNiCuTi<sub>x</sub>/Nb joint

Fig. 8 The SEM image of interface microstructure of ZrB<sub>2</sub>-SiC/Nb joint brazed at 1160°C for 60 min with CoCrFeNiCuTi<sub>x</sub> filler: (a) Ti<sub>0</sub> (b) Ti<sub>0.5</sub> (c) Ti (d) Ti<sub>1.5</sub>

Fig.9 XRD analysis of ZrB<sub>2</sub>-SiC/Nb joint brazed with CoCrFeNiCuTi<sub>x</sub> filler with different Ti content: (a) the reaction layer (b) the center area

Fig.10 Fracture micrographs of the joints brazed at 1160°C for 60 min with CoCrFeNiCuTi<sub>x</sub> filler after the shear test at room temperature or 650°C: (a) and (e) Ti<sub>0</sub>, (b) and (f) CoCrFeNiCuTi<sub>0.5</sub>, (c) and (g) CoCrFeNiCuTi, (d) and (h) CoCrFeNiCuTi<sub>1.5</sub>.

## Tables

Table 1 Results of EDS of CoFeNiCrCuTi<sub>x</sub> (at. %)

Alloy	Spot	Ti	Cr	Fe	Co	Ni	Cu	Possible phase
CoFeNiCrCu	1a	-	22.89	21.85	24.24	20.40	10.61	FCC
	1b	-	2.17	2.26	2.13	6.14	87.31	Cu(s, s)
CoFeNiCrCuTi <sub>0.5</sub>	2a	5.47	22.84	21.30	20.49	17.39	12.51	FCC
	2b	13.56	11.64	13.45	17.06	24.30	20.00	FCC2
	2c	0.23	4.51	4.12		9.02	78.39	Cu(s, s)
	3a	13.87	12.21	13.46	14.99	25.29	20.19	FCC2
CoFeNiCrCuTi	3b	8.16	37.49	23.44	17.79	9.81	3.32	σ
	3c	21.74	14.51	19.06	21.56	17.69	5.44	Rich-Ti Laves
	3d	1.56	2.08	2.99	2.41	3.80	87.16	Cu(s, s)
	4a	2.78	70.01	16.99	7.08	2.21	0.94	Cr
CoFeNiCrCuTi <sub>1.5</sub>	4b	19.15	5.60	7.91	11.12	33.60	22.63	FCC2
	4c	25.46	18.43	21.97	19.70	11.10	3.34	Rich-Ti Laves
	4d	3.67	3.04	3.54	2.94	5.79	81.02	Cu(s, s)

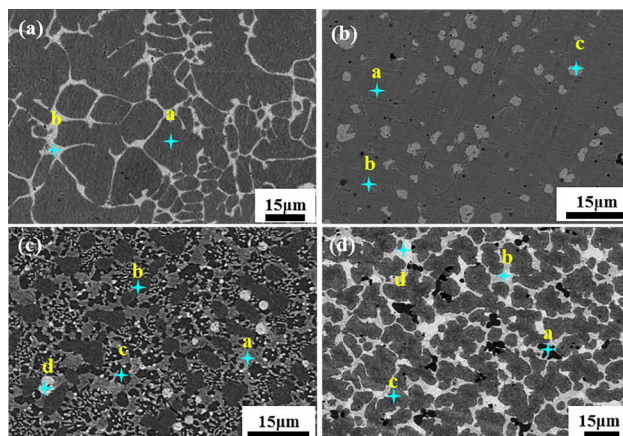
Table 2 Results of EDS at points A~G in Fig. 4 (at. %)

Spot	Zr	Fe	Co	Ni	Cu	B	Cr	Nb	Possible phase
A	0.10	0.44	0.08	0.03	0.59	37.19	61.54	0.04	Cr <sub>2</sub> B
B	0.43	15.67	16.59	16.96	6.09	7.14	12.67	24.45	rich-Nb Laves
C	0.25	27.22	23.24	20.48	12.86	4.35	11.22	0.38	FCC
D	0.39	11.22	3.33	0.67	0.29	27.14	55.21	0.31	(Cr, Fe) <sub>2</sub> B
E	0.08	3.08	2.15	0.92	0.10	29.82	63.08	0.09	Cr <sub>2</sub> B
F	0.08	0.22	8.63	3.46	75.32	7.71	0.93	3.64	Cu(s, s)
G	0.13	3.68	5.23	3.88	0.42	7.11	11.36	64.05	Nb(s, s)

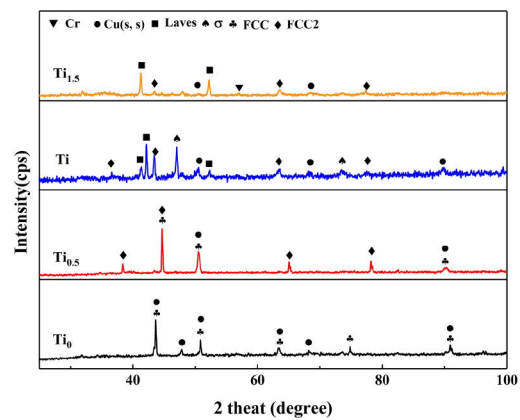
Table 3 Results of EDS at points A~G in Fig. 7 (at. %)

Spot	Zr	Fe	Co	Ni	Cu	B	Cr	Nb	Ti	Possible phase
A	0.16	5.98	4.45	2.91	1.54	38.21	45.07	0.53	1.15	Cr <sub>2</sub> B
B	1.19	2.20	1.13	1.23	1.35	41.91	1.15	8.41	39.24	(Ti, Nb)B
C	0.09	22.78	20.67	19.62	3.05	10.44	15.41	0.60	7.34	FCC

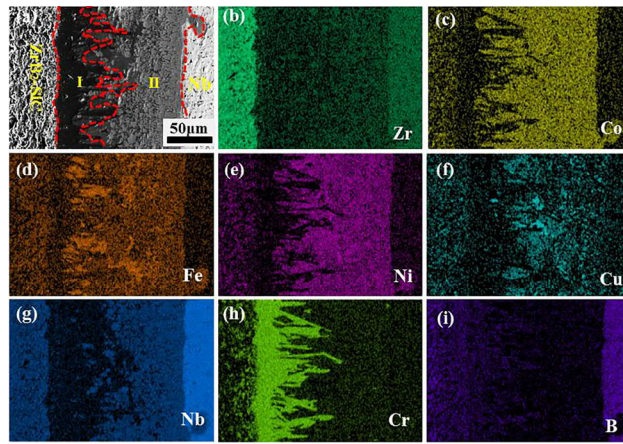
<b>D</b>	<b>1.72</b>	<b>9.45</b>	<b>18.29</b>	<b>16.14</b>	<b>3.66</b>	<b>9.04</b>	<b>12.14</b>	<b>5.77</b>	<b>23.79</b>	<b>rich-Ti Laves</b>
<b>E</b>	<b>0.12</b>	<b>1.54</b>	<b>1.64</b>	<b>2.48</b>	<b>0.10</b>	<b>91.50</b>	<b>0.50</b>	<b>0.44</b>	<b>1.72</b>	<b>Cu(s, s)</b>
<b>F</b>	<b>1.03</b>	<b>1.29</b>	<b>2.50</b>	<b>0.97</b>	<b>1.81</b>	<b>45.90</b>	<b>0.97</b>	<b>8.56</b>	<b>36.97</b>	<b>(Ti, Nb)B</b>
<b>G</b>	<b>0.37</b>	<b>2.23</b>	<b>4.09</b>	<b>3.89</b>	<b>1.63</b>	<b>8.73</b>	<b>1.49</b>	<b>76.46</b>	<b>1.11</b>	<b>Nb(s, s)</b>



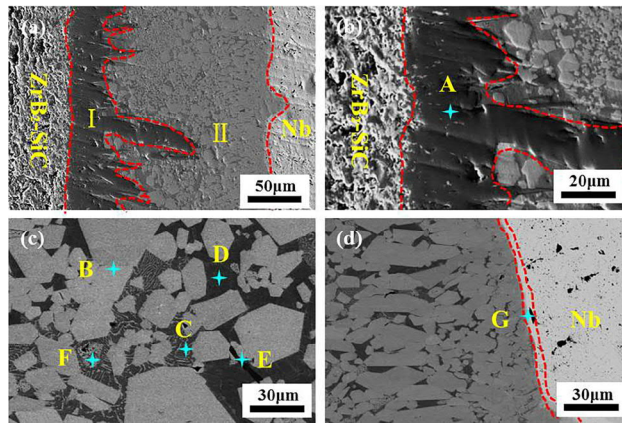
jace\_17732\_f1.jpg



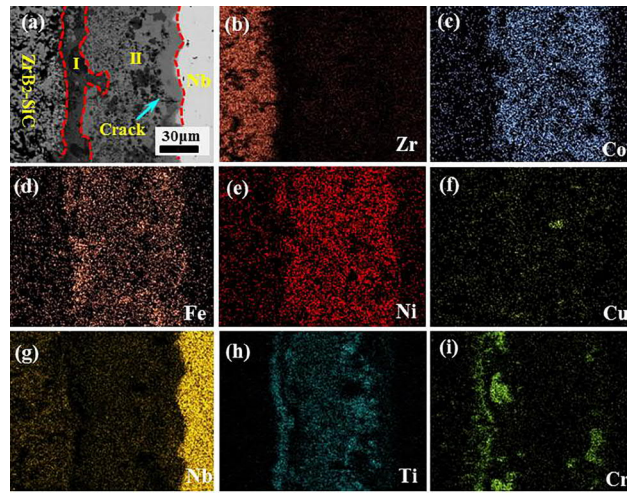
jace\_17732\_f2.jpg



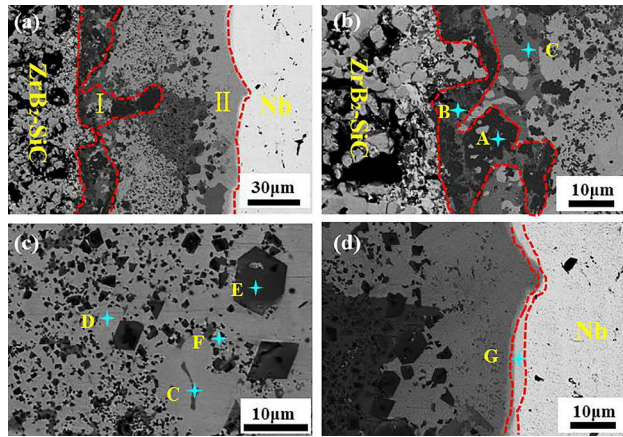
jace\_17732\_f3.jpg



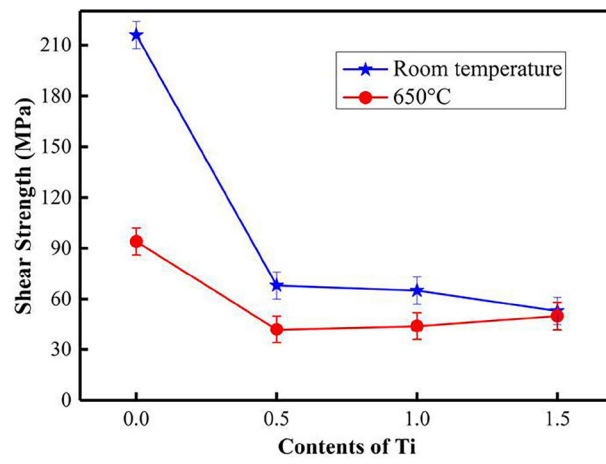
jace\_17732\_f4.jpg



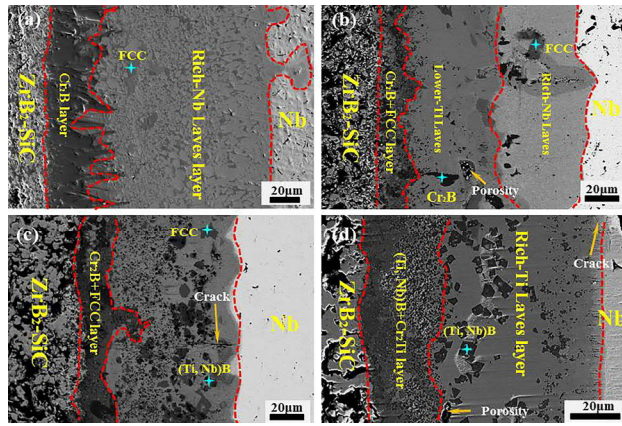
jace\_17732\_f5.jpg



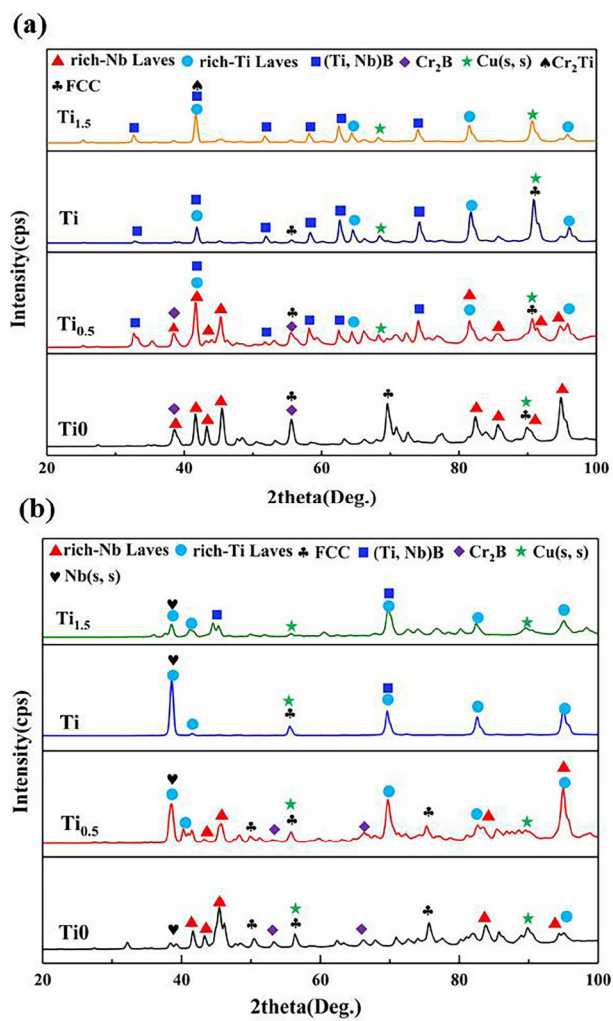
jace\_17732\_f6.jpg



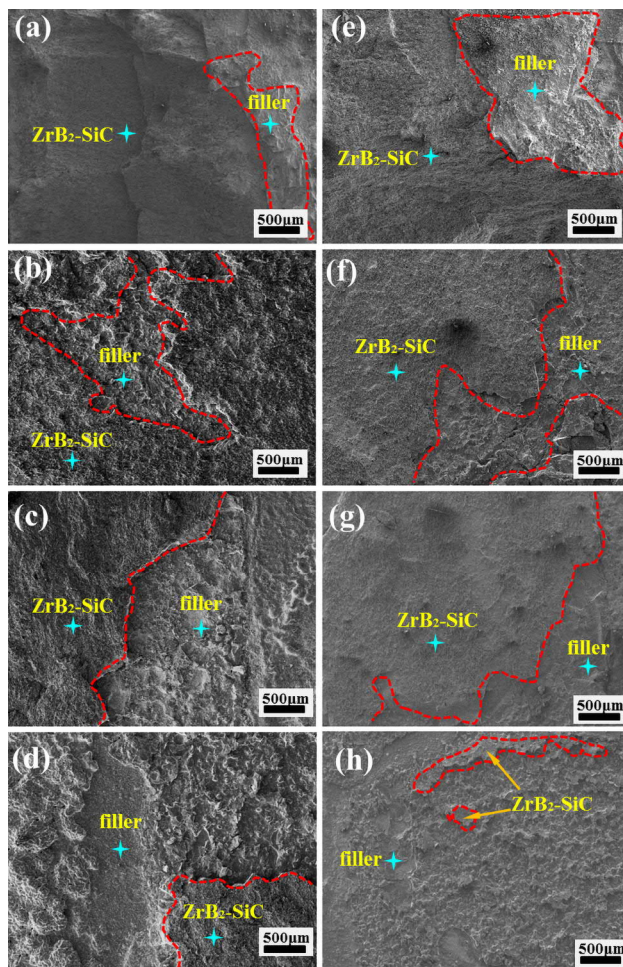
jace\_17732\_f7.jpg



jace\_17732\_f8.jpg



jace\_17732\_f9.jpg



jace\_17732\_f10.jpg